Effects of oligomerization and decomposition to the nanoparticle growth, a model study

Arto Heitto[1], Kari Lehtinen[1,2], Tuukka Petäjä[3], Felipe Lopez-Hilfiker[4,5], Joel A. Thornton[4], Markku Kulmala[3] and Taina Yli-Juuti[1]

5   1 Department of Applied Physics, University of Eastern Finland, 70211 Kuopio, Finland
2 Finnish Meteorological Institute, 70211 Kuopio, Finland
3 Institute for Atmospheric and Earth System Research/Physics, University of Helsinki, 00014 Helsinki, Finland
4 Department of Atmospheric Sciences, University of Washington, 98195 Seattle, WA, USA
5 Present address: Tofwerk AG, 3600 Thun, Switzerland

10   *Correspondence to*: Arto Heitto (arto.heitto@uef.fi)

Abstract. The rate at which freshly formed secondary aerosol particles grow is an important factor in determining their climate impacts. The growth rate of atmospheric nanoparticles may be affected by particle phase oligomerization and decomposition of condensing organic molecules. We used Model for Oligomerization and Decomposition in Nanoparticle Growth (MODNAG) to investigate the potential atmospheric significance of these effects. This was done by conducting multiple
15   simulations with varying reaction-related parameters (volatilities of the involved compounds and reaction rates) using both artificial and ambient measured gas phase concentrations of organic vapors to define the condensing vapors. While our study does not aim at providing information on any specific reaction, our results indicate that particle phase reactions have significant potential to affect the nanoparticle growth. In simulations where one-third of a volatility basis set bin was allowed to go through particle phase reactions the maximum increase in growth rates was 71% and decrease 26% compared to base case where no
20   particle phase reactions were assumed to take place. These results highlight the importance of investigating and increasing our understanding of particle phase reactions.

1 Introduction

Aerosols are ubiquitous in the atmosphere and they affect our climate in multiple ways. Directly they can affect the radiative forcing by reflecting, refracting, and absorbing sunlight, and indirectly by acting as cloud condensation nuclei (CCN) and
25   forming clouds (Boucher et al., 2013). The effect of aerosol-cloud interactions in the Earth's radiative balance is one of the biggest uncertainties we have in recent climate models and studies (IPCC, 7. chapter, Boucher et al., 2013).

For an aerosol particle to act as CCN, it needs to be large enough in size, at least some tens of nanometers in diameter (Pierce and Adams, 2007; Reddington et al., 2017). This can be, on one hand, a limiting factor for climate impacts of small primary aerosols as Aitken-mode sized primary particles such as soot particles are quite often non-hygroscopic, which hinders their
30   activation as CCN (e.g. Zhang et al. 2008, PNAS). However, atmospheric aging typically enhances their solubility and alter

their morphology towards being CCN active (Trischer et al. 2011; Lambe et al. 2015,). On the other hand, the secondary aerosols that are formed in the atmosphere via gas-to-particle conversion (e.g., Kulmala et al. 2014,.) need to undergo substantial growth until they reach sizes relevant for CCN activation (Kerminen et al. 2012). Regardless, it is estimated that approximately half of the particles acting as CCN are formed in the atmosphere by nucleation from atmospheric gases
35 (Merikanto et al., 2009; Paramonov et al. 2015).

Organic molecules play an important role in the early state of the growth of atmospheric particles (Wehner et al., 2005; Kerminen et al., 2012; Kulmala et al., 2013; Shrivastava et al., 2017; Mohr et al., 2019; Yli-Juuti et al., 2020). Gas phase oxidation of volatile organic compounds produces a variety of molecules, some of which condense on particles and form secondary organic aerosol (SOA) (Hallquist et al., 2009). How much a compound contributes to the particle growth is to a
40 large extent controlled by their gas phase concentration and volatility. In recent studies, nanoparticle growth simulated based on the observed organic vapor concentrations and estimated saturation vapor concentrations have been found in fairly good agreement with observed particle growth in an atmospheric environment (Mohr et al., 2019) and in laboratory (Stolzenburg et al., 2018), although uncertainties are associated with both the measured gas phase concentrations and the estimated saturation concentrations.

45 In addition to gas phase reactions, particle phase reactions can increase or reduce the volatility. One pathway for more volatile compounds to affect the growth is by oligomerization in the particle phase (Tolocka et al., 2004; Hall and Johnston, 2012). Studies have reported oligomers are in abundance in SOA and that they may contribute up to 50% of organic mass in them (Gao et al., 2004, Denkenberger et al., 2007; Hall and Johnston, 2011; Kourtchev et al. 2016). In oligomerization two or more smaller molecules combine with each other forming larger oligomer molecules which are likely less volatile, i.e., less likely
50 to evaporate. On the contrary, if a molecule decomposes inside a particle, it breaks down forming new smaller molecules. These molecules tend to have higher volatility than the original molecule and thus may evaporate back to the gas phase hindering the particle growth even if the original molecule would have preferred to stay in the particle phase. Recent studies have reported a wide range of different oligomerization and decomposition rates in multiple reactions. For example, several studies have been conducted optimizing model to measurements using oligomerization and decomposition reactions as fitting
55 parameters. The fitted reaction rates for oligomerization have ranged between 10^{-26} to $2.8 \cdot 10^{-14}$ cm^3 molecule^{-1} s^{-1} (Kolesar et al., 2015; Roldin et al., 2014; Vesterinen et al., 2006) and for decomposition between 10^{-5} to 10^{-2} s^{-1} (Kolesar et al., 2015; Roldin et al., 2014; D'Ambro et al., 2018; Trump and Donahue, 2014). However, as the identities of the organic compounds participating in atmospheric nanoparticle growth are largely unknown or uncertain, there is lack of knowledge on the particle phase reactivity and reaction rates of the molecules in the condensed phase.

60 In this study we use an atmospheric process model to study how the oligomerization and decomposition influence the growth of atmospheric nanoparticles. Particularly, our aim is to explore how much particle phase reactions can affect nanoparticle growth and further to compare these effects with the uncertainties in the ambient and saturation vapor concentrations of the gas phase products. To do this, simulations are first performed based on artificially created but justified gas phase concentrations with a series of assumptions about particle phase reaction properties. These simulations are subsequently used

65 to determine the range of properties on which particle growth is sensitive to. Second, simulations constrained by atmospheric observations are performed in order to estimate the extent to which particle phase reactions can impact particle growth. This will allow us to investigate the sensitivities of predicted growth for reactions and the related properties but will not infer what kind of reactions take place in the atmospheric nanoparticles.

2 Methods

70 ### 2.1 Model description

Model for Oligomerization and Decomposition in NAnoparticle Growth (MODNAG) was developed and used in this study. MODNAG is a single-particle growth model that simulates time-evolution of particle size and composition based on ambient gas phase concentrations of condensing compounds, temperature, and relative humidity (RH). In this study, the system consists of multiple organic compounds, water, sulfuric acid, and ammonia.

75 The organics are divided into four groups (I-IV): three groups (I-III) that condense from the gas phase and one group (IV) that includes oligomerization and decomposition products that are formed in the particle phase during the simulation. The three condensing groups (I-III) all include seven organic compounds which are defined by their saturation concentration (C*) using Volatility Basis Set (VBS, Donahue et al., 2011), where the volatility bins range from C*=10^{-4} µg m^{-3} to C*=10^{2} µg m^{-3}. These three condensing groups (I-III) differ in terms of what kind of reactions they can go through in the particle phase. The organic

80 group I is called non-reactant group and these compounds will not go through any reactions in the particle phase. The compounds in the organic group II, called oligomerization group, can combine with each other in the particle phase forming new compounds, dimers. The compounds in the organic group III, called decomposition group, can fragment into two smaller compounds in the particle phase. The products of the reactions from the oligomerization and decomposition groups form the organic group IV in the model.

85 The change in the mass of compound j in a particle (m_j) is calculated based on the mass flux between gas and particle phase and the oligomerization and decomposition reactions they go through using equation

$$\frac{dm_j}{dt} = 2\pi(d_p + d_j)(D_p + D_j)\beta_{m,j}(C_j - C_{eq,j}) + (P_{olig,j} - L_{olig,j} + P_{dec,j} - L_{dec,j})\frac{M_j}{N_A} \qquad (1)$$

where M_j (kg mol^{-1}) is the molar mass, d_j molecular diameter (m), D_j diffusion coefficient (m^2 s^{-1}), C_j gas phase mass

90 concentration and $C_{eq,j}$ equilibrium mass concentration of compound j respectively (note that both are here converted to units of kg m^{-3}), d_p is the diameter (m) and D_p diffusion coefficient of the particle (m^2 s^{-1}) and N_A Avogadro's constant (mol^{-1}). $P_{olig,j}$ and $L_{olig,j}$ are the production and loss rates by oligomerization and $P_{dec,j}$ and $L_{dec,j}$ are the production and loss rates by decomposition.

The first part on right in Eq. (1) describes the transition regime mass flux of condensation to/evaporation from a particle and

95 is based on the difference in the gas phase and equilibrium concentrations of the compound. β_i is the transition regime

correction factor defined as (Fuchs and Sutugin, 1970):

$$\beta_j = \frac{1 + Kn_j}{1 + (\frac{4}{3\alpha_{m,j}} + 0.377)Kn_j + \frac{4}{3\alpha_{m,j}}Kn_j{}^2} \tag{2}$$

where $\alpha_{m,j}$ is mass accommodation coefficient and Kn_j is the Knudsen number. In our model, for Knudsen number we use

100 (Lehtinen and Kulmala, 2003):

$$Kn_j = \frac{2\lambda_j}{d_p + d_j} \tag{3}$$

where λ_j is the free mean path of the condensing compound j. The mean free path is defined as (Lehtinen and Kulmala,2003):

$$\lambda_j = \frac{3(D_p + D_j)}{\sqrt{c_p + c_j}} \tag{4}$$

105 where c_p and c_j are the mean thermal speed of the particle and condensing compound, respectively. The equilibrium vapor

concentration of j is calculated as

$$C_{eq,j} = \gamma_j \chi_j C^*{}_j \exp\left(\frac{4\sigma v_j}{RTd_p}\right) \tag{5}$$

where γ_j is the activity coefficient, χ_j the mole fraction, $C^*{}_j$ the saturation concentration, v_j the molar volume of compound j, σ

the surface tension of the particle, R the gas constant and T the temperature. In this study we assume an ideal solution and

therefore the activity coefficient γ_j is equal to 1.

110 The second part on the right-hand side of Eq. (1) describes the production and loss of the compound j from oligomerization

and decomposition reactions. $L_{olig,j}$ describes the loss rate of compound j due to oligomerization reactions with other

compounds i ($L_{olig,j} \neq 0$ only for organic group II) and is calculated as

$$L_{olig,j} = k_{olig}N_jN_iV_p \tag{6}$$

where k_{olig} is the oligomerization rate coefficient, V_p the volume of the particle and N_j and N_i the particle phase molecular

115 concentrations of compounds j and i, respectively. $L_{dec,j}$ describes the loss rate of compound j due to decomposition to smaller

molecules ($L_{dec,j} \neq 0$ only for organic group III) and is calculated as

$$L_{dec,j} = k_{dec} N_j V_p \tag{7}$$

where k_{dec} is the decomposition rate coefficient of compound j. $P_{olig,j}$ and $P_{dec,j}$ describe the production of compound j by oligomerization and decomposition, respectively, ($\neq 0$ only for organic group IV) and they are calculated as

$$P_{olig,j} = k_{olig} N_f N_y V_p \tag{8}$$

120

$$P_{dec,j} = k_{dec} N_i V_p \tag{9}$$

where f, y, i indexes describe the two oligomerizing compounds from the group II and the fragmenting compound in the group III, respectively.

Eq. (1) is used both for organics and sulfuric acid. Water is assumed to be constantly in equilibrium between gas and particle

125 phase and the amount of ammonia (by mole) is assumed to equal the amount of sulfuric acid in the particle phase. The model is built with an option of including particle phase acid-base chemistry according to E-AIM (http://www.aim.env.uea.ac.uk; Clegg et al., 1992; Clegg and Seinfeld, 2006a, b; Wexler and Clegg, 2002) similar to MABNAG model (Yli-Juuti et al., 2013). However, here an option of ideal solution assumption without acid-base chemistry was applied as the focus is on the organics, although we acknowledge that acidity can enhance the oligomerization (Tolocka et al, 2004).

130 The particle is assumed to be liquid like and have no particle phase diffusional limitations. The viscosity of the particle has been suggested to possibly have an effect on the particle growth (Virtanen et al., 2010), however the effect may not be significant at atmospheric boundary layer relative humidities at least at warm environments (Renbaum-Wolff et al., 2013; Yli-Juuti et al., 2017; Li et al., 2019), and here such effect was neglected to focus on oligomerization and decomposition.

135 **2.2 Simulation setup**

In MODNAG it is possible to include multiple oligomerization and decomposition reactions in the same simulation. In recent studies it has been shown that oligomerization is often reversible (Trump and Donahue, 2014). In our simulations we have mostly assumed irreversible reactions but conducted simulations with reversible oligomerization for few example cases to explore potential influence of this process. Also, for simplicity we have assumed that only one reaction happens at a time and

140 that it happens only between two compounds, although in reality the reaction chains are observed to be longer and include multiple reactions and compounds (Tolocka et al.,2004, Kolesar, Heaton et al., 2007). In all simulations the initial particle diameter was 2 nm, and it consisted solely of sulfuric acid.

Our analysis included "oligomerization simulations" and "decomposition simulations". In the oligomerization simulations one pair of compounds in organic group II was allowed to react and form a dimer. Other compounds in group II and all

145 compounds in group III were assumed to be non-reactant similarly to group I compounds. We run such simulations for reactions between all possible compound pairs in organic group II. For each pair of reacting compounds, several simulations

were run by assuming the product to have a saturation concentration between $C^*=10^{-6}$ µg m^{-3} and 10^1 µg m^{-3}, however the volatility of the product was restricted to be always at least one order of magnitude lower than the volatility of the less volatile reacting compounds. For each combination of the pair of reacting compounds and C^* of the product, the analysis included
150   simulations where oligomerization rate coefficient k_{olig} ranged from 10^{-27} m^3 s^{-1} to 10^{-18} m^3 s^{-1}. Sensitivity tests showed that with higher or lower oligomerization rate coefficients there were not any significant changes in the results compared to these upper and lower limits, respectively.

In the decomposition simulations the initial compound from organic group III fragments forming two smaller product compounds. These two product compounds could be identical or have different properties. Other compounds in group III and
155   all compounds in group I and group II were assumed to be non-reactant. For each decomposing compound from organic group III, simulations were run with volatilities of the product compounds ranging from $C^*=10^{-3}$ µg m^{-3} to 10^2 µg m^{-3}. The volatility of each product compound was limited to be always at least one order of magnitude higher than the initial compound's volatility. For each combination of the initial compound and the pair of product compounds, simulations were run with decomposition rate coefficient k_{dec} ranging from 10^{-5} s^{-1} to 1 s^{-1}.

160   In the simulations with reversible reaction oligomerization of compounds was done similarly as in irreversible oligomerization simulations described above, with the exception where the formed oligomers could decompose back to their initial group II bins after oligomerization. Ranges for k_{olig} and k_{dec} were similar to the irreversible reactions.

The total gas phase concentration of compounds in different VBS bins was divided evenly between groups I, II and III, which means, that one-third of a bin was reacting in a given simulation. We chose this in order to investigate effects of particle phase
165   reactions in a more moderate case compared to assuming that all or majority of the compounds of any volatility would undergo reactions. An assumption for this was required since relevant particle phase reactions of organics are not well known. We tested the sensitivity of results to this assumption by performing additional simulations with the assumption that all molecules of a bin can react (see Results, Sect. 3.2).

In this study the aim was to get an overview of how much oligomerization and decomposition can affect the growth of
170   atmospheric nanoparticles. For this, the above sensitivity runs were performed for two scenarios being representative of environments where the nanoparticle are growing. In Case 1, an artificial gas phase composition was given as an input to the model. The vapor concentrations were selected in a way that vapor concentrations and the resulting particle growth rates are of similar magnitude as observed in the boreal forest atmosphere (Mohr et al., 2019). Additionally, the less volatile organic compounds were set to have lower concentrations compared to the more volatile compounds following atmospheric
175   observations but in a simplified way (Mohr et al., 2019). Properties of the seven model compounds (VBS bins) in all condensing groups (I-III) are illustrated in Table 1. In addition, we have 280 product compounds (group IV). Here the diffusivity is assumed to be similar with condensing components in similar volatility bin. For oligomerization product compounds the molar mass of the compound was the sum of molar masses of reacting compounds, and for decomposing product compounds the molar masses were calculated by dividing the molar mass of decomposing compound relative to the
180   logC* of the product compounds.

Table 1: The properties of organic model compounds in groups I, II and III, for Case 1, where the properties are artificial, mimicking atmospheric conditions. C* is saturation concentration, M molar mass, D particle phase diffusion coefficient and C gas phase concentration. C* is expressed both in units of μg m^{-3} and molec cm^{-3}.

Compound	C* (μg m^{-3}) / (molec cm^{-3})	M (kg mol^{-1})	D (m^2 s^{-1})	C (molec cm^{-3})
bin 1	10^2 / 3.17×10^{11}	0.190	5×10^{-6}	1.67×10^7
bin 2	10^1 / 2.74×10^{10}	0.220	5×10^{-6}	1.67×10^7
bin 3	10^0 / 2.51×10^9	0.240	5×10^{-6}	1.67×10^7
bin 4	10^{-1} / 2.32×10^8	0.260	5×10^{-6}	3.33×10^6
bin 5	10^{-2} / 2.01×10^7	0.300	4×10^{-6}	3.33×10^6
bin 6	10^{-3} / 1.82×10^6	0.330	4×10^{-6}	3.33×10^6
bin 7	10^{-4} / 1.63×10^5	0.370	4×10^{-6}	3.33×10^6

185

In Case 2, simulations were run with gas composition more directly restricted by atmospheric observations. Vapor concentrations and molecular composition measured with a chemical ionization mass spectrometer at Hyytiälä measurement station (Mohr et al., 2019) in spring 2014 during a new particle formation (NPF) event were grouped in a VBS based on their

190   C* estimated with the parameterization by Li et al. (2016) and temperature dependence of C* estimated based on the method by Epstein et al. (2010). This VBS representation of the gas concentrations of the organics was used as an input for the model. The measured gas phase concentrations were assigned evenly for the organic groups I, II, and III, but since only one oligomerization or decomposition reaction was allowed in a simulation, most of the concentration was not reacting, except for the one-third of a bin assigned to reacting organic group II or III compounds to investigate oligomerization or decomposition,

195   respectively. The observational data used here are presented in Mohr et al. (2019) where particle growth was simulated based on the observed gas phase concentrations without considering particle phase oligomerization or decomposition of organic compounds. In these simulations, we used averages over the detected NPF event for ambient conditions and properties (M$_j$ and D$_j$) of model compounds (VBS bins) were calculated as gas phase mass concentration weighted averages of organic compounds grouped to each model compound. The properties of model compounds in these Case 2 simulations are listed in

200   Table 2. The properties for group IV compounds were defined similarly to Case 1.

205

Table 2: The properties of model compounds in groups I, II and III, for Case 2. Concentrations are from measurements of Mohr et al. (2019). Saturation concentrations at 300 K (C_{300}*) are calculated using parametrization by Li et al. (2016) and converted to the ambient temperature in the model based on temperature dependence by Epstein et al. (2010). M is molar mass, D particle phase diffusion coefficient and C gas phase concentration.

Compound	C_{300}* (µg m^{-3}) / (molec cm^{-3})	M (kg mol^{-1})	D (m^2 s^{-1})	C (molec cm^{-3})
bin 1	10^2 / $3.04*10^{11}$	0.198	$5.51*10^{-6}$	$7.10*10^6$
bin 2	10^1 / $2.77*10^{10}$	0.217	$5.20*10^{-6}$	$5.90*10^6$
bin 3	10^0 / $2.51*10^9$	0.240	$5.06*10^{-6}$	$3.97*10^6$
bin 4	10^{-1} / $2.35*10^8$	0.256	$5.00*10^{-6}$	$2.85*10^6$
bin 5	10^{-2} / $2.08*10^7$	0.290	$4.56*10^{-6}$	$1.83*10^6$
bin 6	10^{-3} / $1.86*10^6$	0.323	$4.26*10^{-6}$	$1.41*10^6$
bin 7	10^{-4} / $1.60*10^5$	0.376	$3.99*10^{-6}$	$2.61*10^6$

210

3 Results and discussion

3.1 Simulations based on artificially generated gas phase concentrations

The particle growth in simulations with artificially generated gas phase concentrations (Case 1) are presented in Figure 1. In
215 general, our results show that oligomerization increases, and decomposition decreases the particle growth rate. At maximum, the growth rate was increased 139% by oligomerization and decreased 20% by decomposition. In some simulations the growth rate is decreased also by oligomerization. These are simulations where two low volatile (C* < 10^{-2} µg m^{-3} model compounds are forming a dimer and the product is only one order of magnitude less volatile than the initial compounds. In this situation, due to small difference in volatilities between the reacting monomers and the product dimer and zero gas phase concentration
220 of the product compound, the evaporation rate of product compound exceeds the enhancement of condensation due to oligomerization.
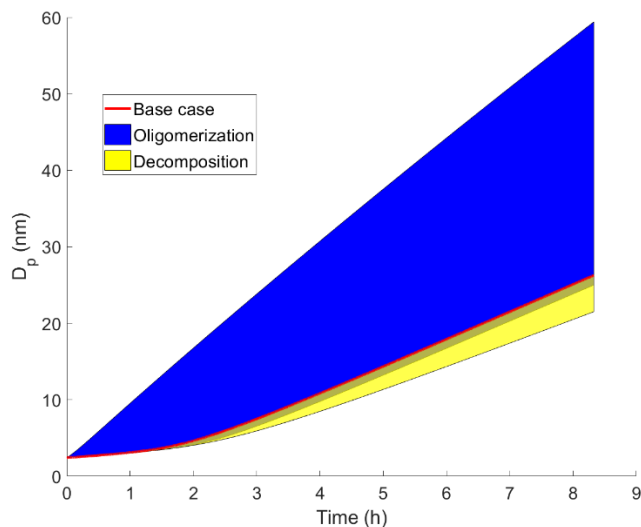
Figure 1: Diameter of the growing particle as a function of time in simulations based on artificial gas phase
concentrations (Case 1 simulations). Red line shows the base case simulation where no particle phase reactions were
allowed. The blue area shows the contribution of oligomerization to the growth, i.e. the envelope of the simulations
where oligomerization was allowed. The yellow area shows the contribution of decomposition to the growth, i.e. the
envelope of the simulations where decomposition was allowed.

The effects of different parameters to the growth with oligomerization can be seen in Figure 2, where simulations with different oligomerization rate coefficient (Fig. 2 a, b), saturation concentrations of oligomerization product (Fig. 2 c, d) and saturation concentration of one of the oligomerizing compounds (Fig. 2 e, f) are presented. Each subfigure shows the base case simulation with no reactions (red dashed line) and the simulation with the fastest growth, where compounds from bins 2 ($C^* = 10^1$ µg m^{-3}) and 3 ($C^* = 10^0$ µg m^{-3}) form a compound with two orders of magnitude lower saturation concentration than in bin 7 ($C^* = 10^{-6}$ µg m^{-3}) with oligomerization rate coefficient k_{olig} of 10^{-18} m^3 s^{-1} (black dashed line). Growth rate (GR) is the changing rate of the particle diameter and it was calculated based on differences in simulated diameter between each time step. The growth rates increase with increasing k_{olig} and with decreasing volatility of oligomerization product. Generally, the growth rate also increases with increasing volatility of oligomerizing compounds. However, with very high volatilities ($C^* > 10^0$ µg m^{-3}) the tendency of these compounds to evaporate can hinder the oligomerization reaction. Also, if two compounds from same bin react, the growth is hindered for two reasons: 1) total gas phase concentration of reacting compounds is lower (one-third of one bin) than in the case of compounds of different bins reacting with each other (one-third of each bin) and 2) the particle phase concentration reduction due to oligomerization is greater than in simulations with reactive compounds from two separate bins.
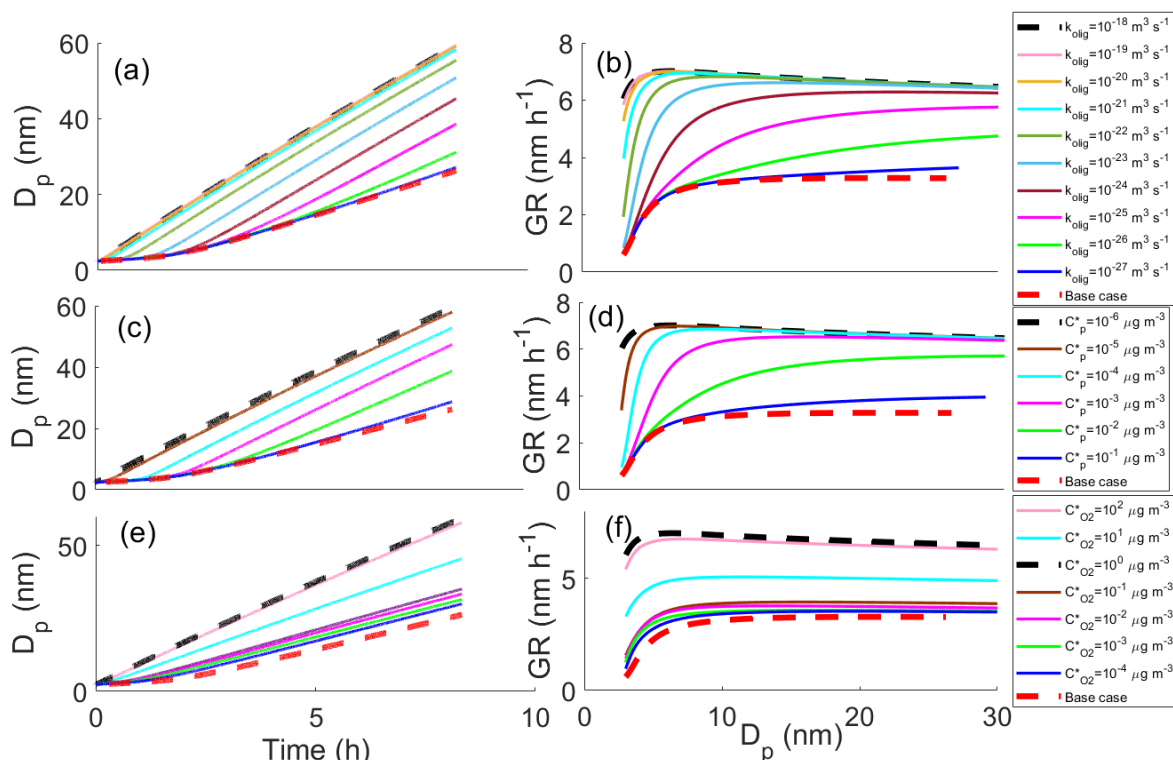
Figure 2: Diameter of the particle (D_p) as a function of time and growth rate of the particle (GR) as a function of diameter in simulations where two model compounds oligomerize forming new oligomerization product, (a, b): for simulations with different oligomerization rate coefficients, (c, d): for simulations with different saturation concentrations of oligomerization product compounds (C^*_p), (e, f): for simulations with different saturation concentrations of one of the oligomerizing compounds (C^*_{O2}). Except for the parameter that was varied, values were as follows: $k_{olig} = 10^{-18} \text{ m}^3 \text{ s}^{-1}$, $C^*_p = 10^{-6} \text{ µg m}^{-3}$, $C^*_{O2} = 10^0 \text{ µg m}^{-3}$ and the saturation concentration of the other reacting compound $C^*_{O1} = 10^1 \text{ µg m}^{-3}$. These parameter values correspond to the simulation with the fastest growth among the Case 1 simulations which is present in every subfigure as black dashed line. The base case simulation in each subfigure describes simulation without oligomerization reaction.

All parameters discussed above, oligomerization rate coefficient and volatility of oligomerizing and product compounds, have clear effect on particle growth. However, their effect is dependent on each other which will be discussed below.

Wang et al. (2010) concluded that oligomerization is nearly inhibited for small particles (< 4nm), because oligomerization is highly dependent on particle phase concentrations, which are very low in the small particles. This is the case also in our study for some of the simulations, as indicated by the small difference in GR between various simulation and the base case simulation particularly for the size below 5 nm (Fig. 2). However, when k_{olig} and difference in volatilities of oligomerizing and product compounds are large enough, oligomerization affects the growth of even the sub-5 nm particles based on our simulations.

When interpreting our simulation results for the small particle sizes it should be noted, that the initial assumption of particle containing only sulfuric acid may affect the results at the beginning of the simulation. As the initial particle contains no organics, some organics will condense in the particle fast during the first-time steps (due to the solution effect in C_{eq}) causing artificially high GR for the beginning of the simulation. For this reason, in Figs 2 b, d and f we present the GR only after the

265 diameter reaches 3 nm. At this point the mass of the particle is about twice the initial mass.

Figure 3 shows effects of different parameters to the particle growth in simulation where decomposition is allowed. Simulations with different decomposition rate coefficient (Fig. 3a, b), saturation concentrations of decomposing compound (Fig. 3c, d), and saturation concentrations of one product compound (Fig. 3e, f) are shown. Each subfigure shows the base case simulation (no reactions, red dashed line) and the simulation with the slowest growth, where compound from bin 7 ($C^* = 10^{-6}$ µg m^{-3})

270 decomposes into two product compounds in bin 1 ($C^* = 10^2$ µg m^{-3}) with decomposition rate coefficient k_{dec} of 1 s^{-1} (black dashed line). Our results show that all varied parameters affect the growth of the particle. For k_{dec} the effect is quite straightforward; with increasing k_{dec}, the growth rate is decreased. The growth rate slows down with a decreasing C^* of decomposing compound due to larger contribution of lower volatility compounds to the particle growth and with an increasing C^* of the product as a consequence of the product evaporating faster for the higher C^* compounds.

275
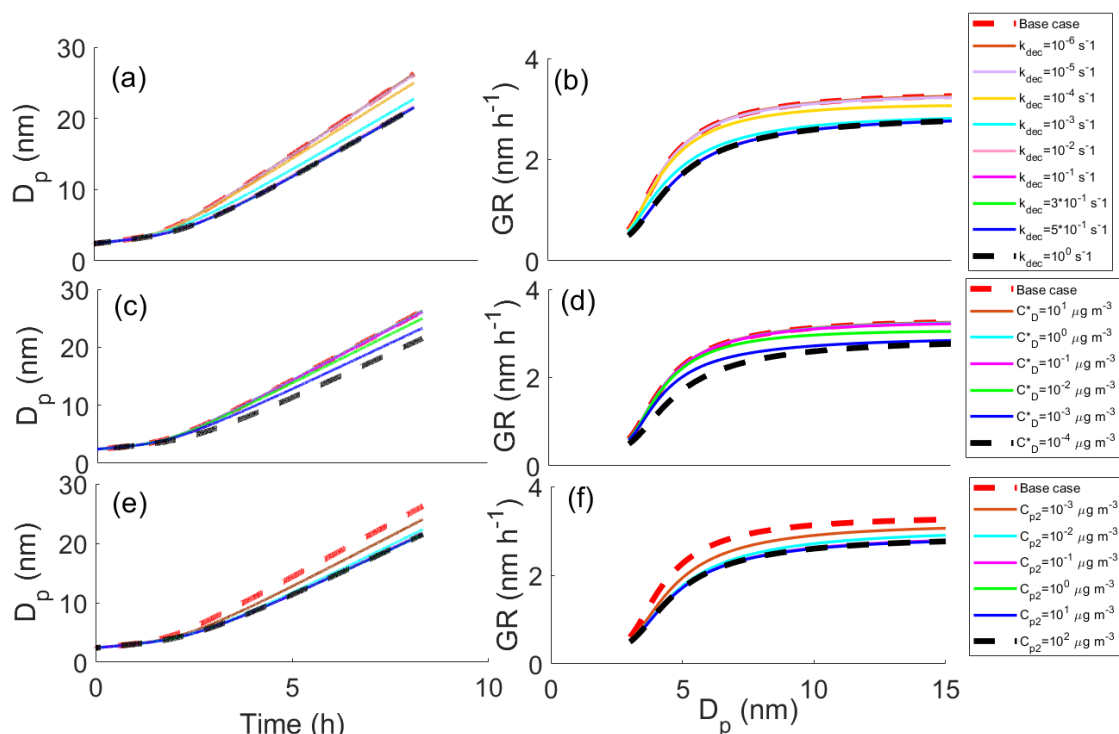
Figure 3: The diameter of the particle (D_p) as a function of time and growth rate (GR) of the particle as a function of diameter in simulations, where one model compound is allowed to decompose into two smaller compounds, (a, b): for simulations with different decomposition rate coefficients, (c, d): for simulations with different saturation concentrations of decomposing compound (C^*_D), (e, f): for simulations with different saturation concentrations of one of the decomposed product compounds (C^*_{p2}). Except for the parameter that was varied, values were as follows: $k_{dec} = 1\ s^{-1}$, $C^*_D = 10^{-4}\ \mu g\ m^{-3}$, $C^*_{p2} = 10^2\ \mu g\ m^{-3}$ and the saturation concentration of the other product compound $C^*_{p1} = 10^2\ \mu g\ m^{-3}$. These parameter values correspond to the simulation with the slowest growth among the Case 1 simulations which is present in every subfigure as black dashed line. The base case simulation in each subfigure describes simulation without decomposition reaction.

In Figure 4 we present the growth rate of the particle in all different simulations with oligomerization for particles under 5 nm in diameter (Fig 4a) and over 5 nm in diameter (Fig 4b). Each colored dot represents one simulation, and the color describes the growth rate. Growth rates are calculated by fitting a straight line in diameter as a function of time, i.e. assuming linear growth. This is important to notice especially with particles under 5 nm in diameter for in that size range the growth is not usually linear (see Fig. 2 and 3). From left to right the subplots show simulations with increasing k_{olig} and from top to bottom decreasing saturation concentration of the product compound formed in the oligomerization reaction. In each subplot on the y- and x-axis are the saturation concentrations of the oligomerizing compounds.
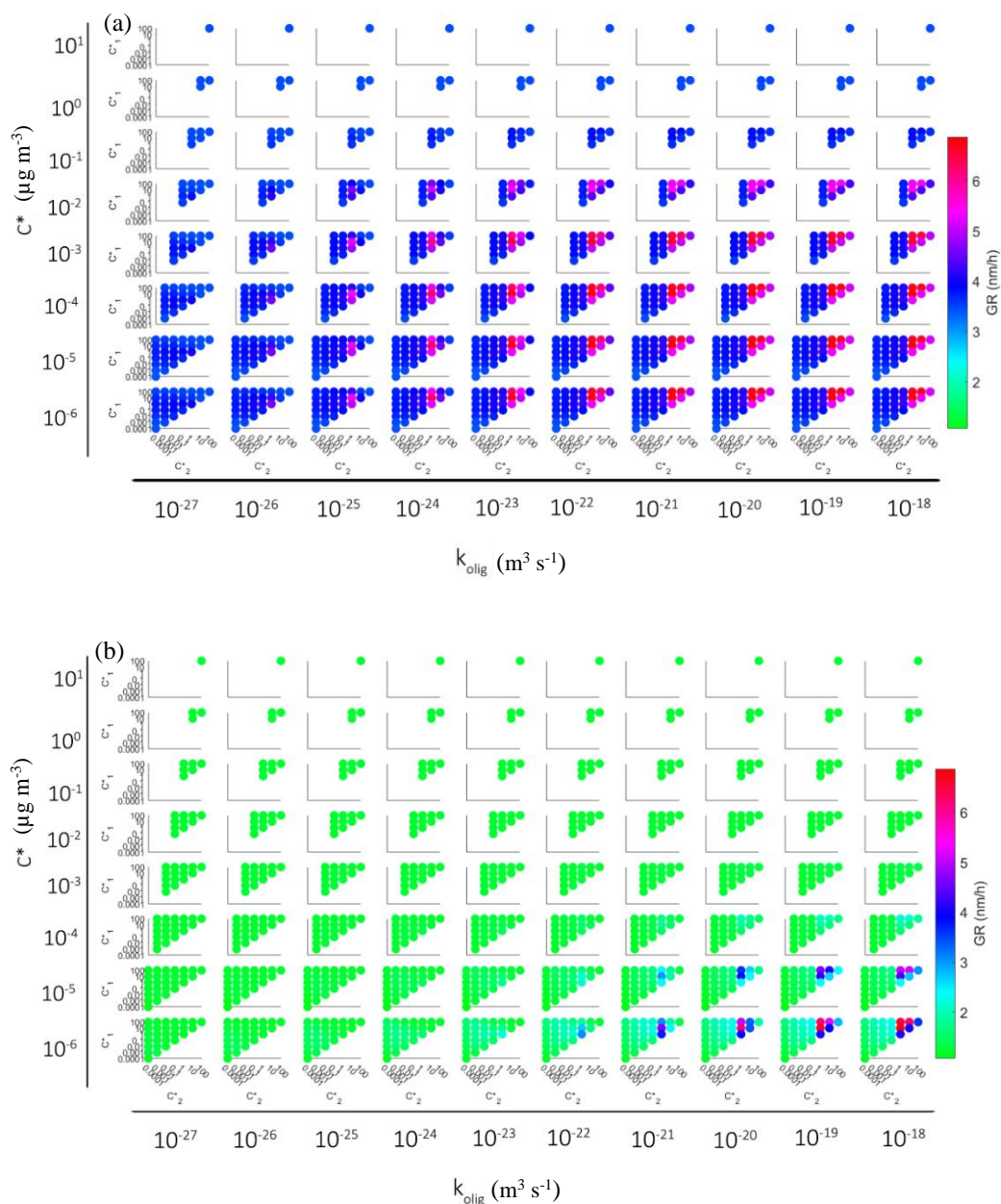
295

Figure 4: Growth rate of the particle in simulations with oligomerization for a) particles over 5 nm in diameter and b) particles under 5 nm in diameter. Each dot describes one simulation, and the color the corresponding growth rate. The growth rates are calculated assuming linear growth curve. In smaller figures the axes describe saturation concentrations of oligomerizing model compounds (µg m⁻³). The wider horizontal axis describes the oligomerization

300 **rate coefficient in the simulation and the vertical axis the saturation concentration of forming oligomerization product.**

For small values of k_{olig} ($< 10^{-24}$ m^3 s^{-1}) the increase in growth rate due to oligomerization is small, especially for under 5 nm particles, where any notable increase can be seen only after $k_{olig} > 10^{-24}$ m^3 s^{-1}. Even for simulations where the most volatile compounds in our setup (bin 1 and 2) oligomerize, growth does not increase much with these low k_{olig}, since compounds that

305 condense to the particle phase will evaporate back to the gas phase before they have time to form less volatile product compounds. With larger k_{olig} however, oligomerization happens so fast that even these higher volatility molecules will oligomerize before evaporation. Without oligomerization reaction these compounds would not contribute to the growth almost at all, so with their oligomerization the growth is enhanced greatly. The gas phase concentrations of three higher volatility compounds are higher than those of lower volatility compounds, which enhances the growth rates even further in simulations

310 where oligomerization takes place between high volatile compounds.
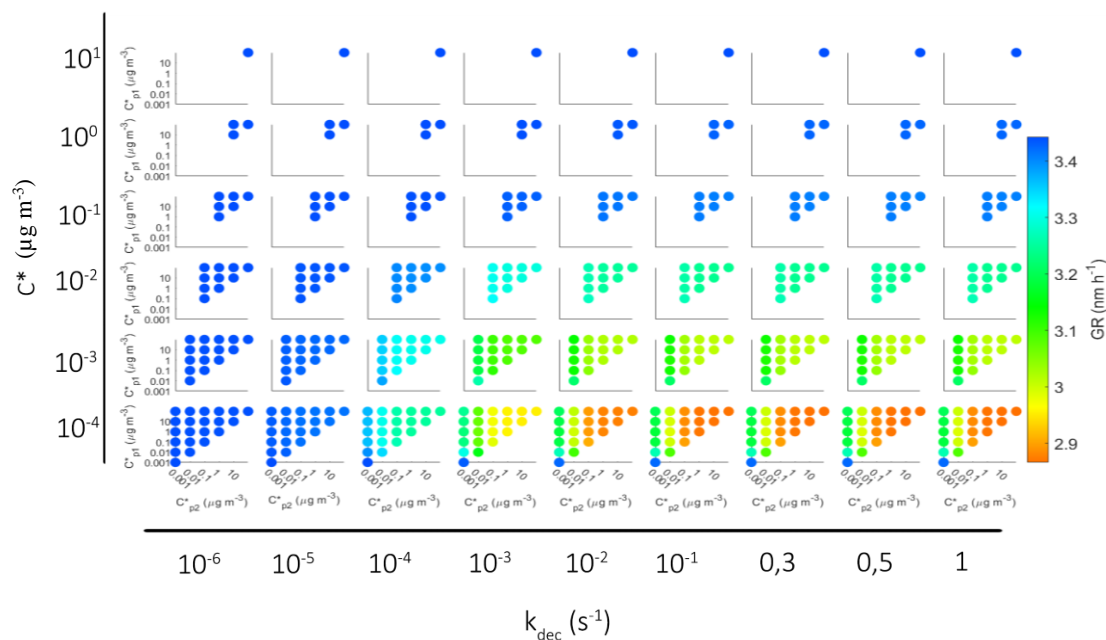
Figure 5: Growth rate of the particle in simulations with decomposition reaction for particles over 5 nm in diameter. Each dot describes one simulation, and the color the growth rate. Growth rates are calculated assuming linear growth curve. In smaller figures the axes describe saturation concentrations of compounds formed by decomposition. The

315 **wider horizontal axis describes the decomposition rate coefficient in the simulation and the vertical axis the saturation concentration of decomposing model components.**

Similar to the Figure 4 for oligomerization reactions, in Figure 5 we present the growth rate of the particle in all different simulations with decomposition, for particles over 5 nm. We have excluded the results for particles under 5 nm in diameter,

320 because for particles under 5 nm decomposition causes little effect on growth. Again, each colored dot represents one simulation, and the color describes the average growth rate during the simulation. The subplots are arranged so that from left to right we have simulations with increasing k_{dec} and from top to bottom decreasing saturation concentration of the decomposing compound. In each subplot the y- and x-axis are the saturation concentration of the end products of decomposition reaction.

325 A clear result here is that the decomposition decreases the GR across the board. In more details, with a small k_{dec} ($< 10^{-4}$ s^{-1}) the decomposition does not affect the growth, since the rate of reactions is slow compared to the condensation mass flux and therefore only a relatively small fraction of molecules reacts. The decomposition starts to have an impact if k_{dec} is at least 10^{-4} s^{-1} and the impact is dependent on the volatilities of the decomposing compound and the product compounds. If decomposing compound is one of the most volatile compounds in our setup, i.e., from three most volatile bins with C* $> 10^{-1}$ µg m^{-3}, the

330 effect of decomposition on GR is very small, because of their low contribution to particle mass. Instead, if the decomposing component is from least volatile bin (C* $= 10^{-4}$ µg m^{-3}), the effect on GR is large, even if the C* of the product compounds would be as low as 10^{-2} µg m^{-3}.

In most of our simulations and in all the results presented this far, the oligomerization and decomposition reactions are assumed to be irreversible. In Figure 6 we present a few cases, where we tested the effect of reversible reactions.

335 In subfigures a, c, e and g (Reaction A) compounds from two most volatile bins (1 and 2, C*= 10^2 µg m^{-3} and 10^1 µg m^{-3} respectively) form an ELVOC (bin 7, C*=10^{-4} µg m^{-3}) and in subfigures b, d, f and h (Reaction B) compounds from bin 2 and 5 (C*=10^1 µg m^{-3} and 10^{-2} µg m^{-3}) form a similar ELVOC as in the left-hand side reactions (bin 7, C*=10^{-4} µg m^{-3}). In both cases the oligomerization product can decompose into the initial compounds. In Reaction A the effect of oligomerization is large, since without it the reacting compounds would contribute to the growth very little. In Reaction B the effect of

340 oligomerization is smaller, for especially the low-volatile reacting compound would condense to the particle phase even without oligomerization. It is worth noting that the difference in gas phase concentrations between higher and lower volatility bins also contributes to the extent that the oligomerization enhances the growth rate. In Reaction B the effect of reversibility is seen only with small values of oligomerization rate coefficients ($k_{olig} < 10^{-23}$ m^3 s^{-1}) while in Reaction A the effect of different decomposition rate coefficients can be seen already with larger values of oligomerization rate coefficients ($k_{olig} > 10^{-18}$ m^3 s^{-1}

345). In reaction B the reversibility of the reaction has less effect on the growth because lower volatility reacting compound tends to stay in the particle phase and thus helps driving the oligomerization reaction.
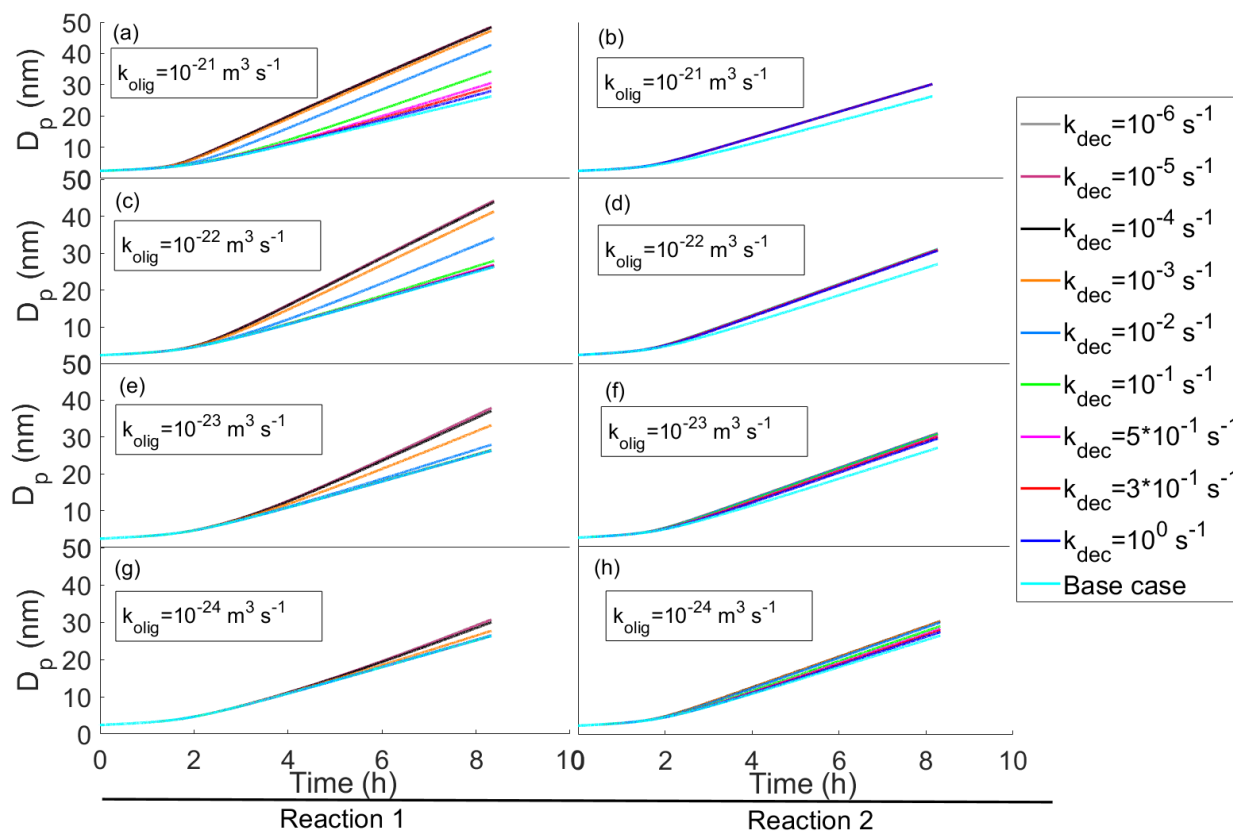
Figure 6: Diameter of the particle as a function of time with reversible oligomerization reactions with different oligomerization and decomposition reaction rates. In each subplot simulations with same oligomerization reaction rate and with different decomposition reaction rates is presented. The oligomerization reaction rates decrease when ascending with subplots. On the left column of subplots (a, c, e and g) the simulations have reaction where two SVOC compounds from the two highest volatility bins (1 ad 2) form an ELVOC (bin 7) and on the right column of subplots (b, d, f and h) the simulations have reaction where a SVOC and LVOC compound (bins 2 and 5) form an ELVOC (bin 7).

3.2 Simulations based on measured gas phase concentrations

Here we explore the thermodynamic parameters in the model and contrast the results to observations in an aerosol formation event observed at Station for Measuring Ecosystem-Atmosphere Relations (SMEAR-II, Hari and Kulmala, 2005) in Hyytiälä,

Finland. Nanoparticle growth after nucleation has been extensively studied at Hyytiälä and nanoparticle GR is relatively well characterized there. At this location, GR values ranging from below 1 nm h^{-1} to several tens of nm h$^-$ have been observed (Dal Maso et al., 2005; Yli-Juuti et al., 2011) average GR for 3-25 nm particles being 2.5 nm h^{-1} (Nieminen et al., 2014). While sub-20 nm particle composition measurements are missing, seasonal variation of GR with maximum in summer indicates

365   importance of organic vapors with biogenic origin (Dal Maso et al., 2005; Yli-Juuti et al., 2011). The importance of organics is supported, e.g., by the positive correlation found between GR of 7-20 nm particles and monoterpene concentration (Yli-Juuti et al., 2011). Further, sulfuric acid condensation can explain only a small fraction of particle growth even down to sub-3 nm size range (Nieminen et al., 2014; Yli-Juuti et al., 2016) and the composition observations of 20 nm particles indicate that organics would cover more than half of particle mass growth (Pennington et al., 2013). On the other hand, GR of particles has

370   been observed to increase with particle size and GR of sub-3 nm particles does not exhibit similar seasonal variation as GR of larger particles which together suggest that there may be different factors affecting growth at different sizes (Yli-Juuti et al., 2011). Particle growth model constrained by observed gas phase concentration of organics captures the observed growth rate fairly well without need for assuming particle phase reactions (Mohr et al., 2019). However, due to uncertainties in gas phase concentrations and properties of organics, possibility of particle phase reactions cannot be completely overruled. Ehn et al.

375   (2007) observations behind a thermodenuder determined size distributions showed that the growth rate was one-third of the GR measured with a normal DMPS-system. Based on a long-term volatility measurements, Häkkinen et al. (2012) found out that soot is not able to explain the residual in the particulate phase and speculated for oligomerization to contribute to the non-volatile cores of nanoparticles growing in the boreal environment.

An evolution of aerosol number size distribution in Hyytiälä on 23.4.2014 is presented in Fig. 7. The observed growth rate was 1.7 nm h^{-1}. In the subsequent simulations we explored the capability of the model and parameter selection to explain the

380   observed aerosol growth in the boreal environment.

Growth of the particle in simulations with measured gas phase concentrations (Case 2) can be seen in Figure 7a. The blue area envelopes simulation results with oligomerization reaction and yellow area envelopes simulation results with decomposition reaction. Without oligomerization the growth in the model is slower than the observed growth (GR in base case simulation

385   1.54 nm h^{-1}, observed GR 1.7 nm h^{-1}). When oligomerization is allowed in the model, it is possible to reach similar GR as observed. However, this can be achieved with multiple combinations of parameters, and therefore it would be challenging to try to estimate what kind of reactions take place in the growing particles by optimizing the model respect to the observed growth. For example, fitting growth rate can be achieved with simulation where compounds from bin 3 and bin 7 form an ELVOC (C* = 10^{-6} µg m^{-3}) with oligomerization rate coefficient of 10^{-27} m^3 s^{-1} and also with simulation where two compounds

390   from bin 1 form a LVOC (C* = 10^{-2} µg m^{-3}) with oligomerization rate coefficient of 10^{-19} m^3 s^{-1}. Similar problem has also been noted by Roldin et al. (2014) when analyzing particle evaporation in laboratory and by Trump and Donahue (2014) when comparing their model to the SOA formation measurements by Presto and Donahue (2006).
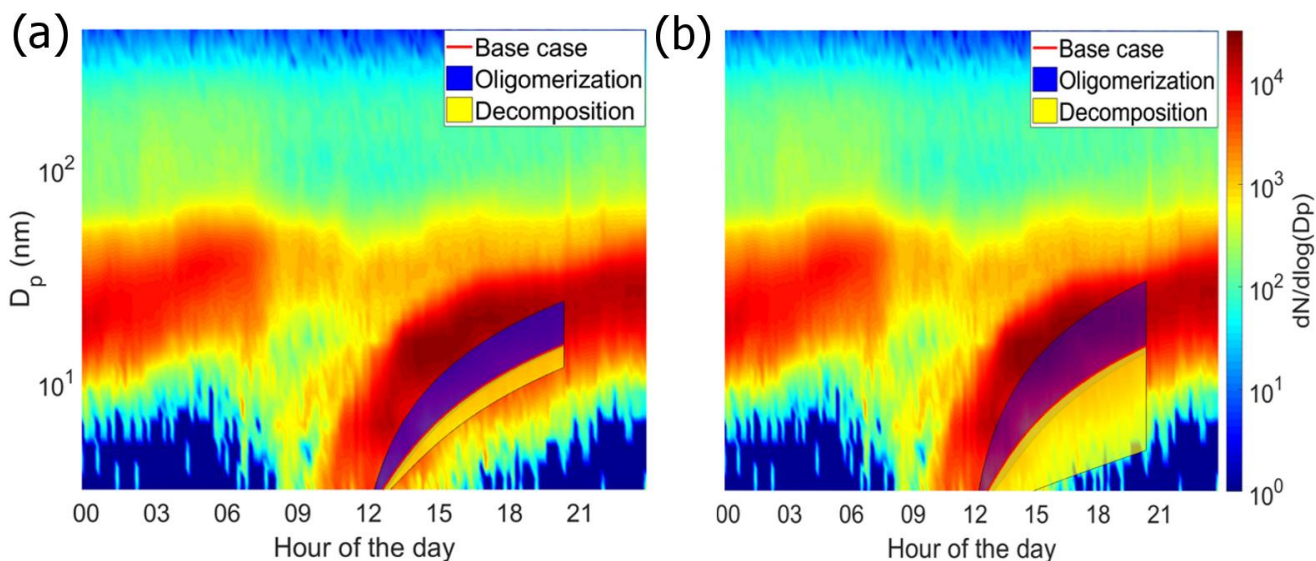
Figure 7: Observed particle size distribution and the model results on diameter of the particle as a function of time in simulations based on measured gas phase concentrations. Base case simulation with no reactions is shown with red line. The blue area shows the possible contribution of oligomerization to the growth, i.e. the envelope of the simulations where oligomerization was allowed. The yellow area shows the possible contribution of decomposition to the growth, i.e. the envelope of the simulations where decomposition was allowed. The measured particle size distribution is shown in the background. a) Model simulations where 1/3 of VBS bin was allowed to react. b) Model simulations where whole VBS bin was allowed to react.

Uncertainties in saturation concentrations of organic compounds are another issue that makes it difficult to approximate which of the assumed oligomerization reactions would fit best with the observed growth. In this study, we used the parametrization of Li et al. (2016) to calculate the C^* values based on molecular formula. Multiple other parametrizations have also been proposed (e.g., Donahue et al., 2011; Stolzenburg et al., 2018; Mohr et al., 2019) and these lead to somewhat different simulated growth rates (Mohr et al., 2019). It should be noted that while the observational data used here was part of the analysis in Mohr et al. (2019), a different C^* parametrization was used there as the base case and with that parameterization the growth was overestimated even without any particle phase reactions. Overall, the C^* values of organics can vary over several orders of magnitude between different calculation methods (Mohr et al., 2019). Therefore, the reaction that would produce the best fit between observed and simulated GR may vary from oligomerization to decomposition between the different C^* parameterizations.

In the results presented so far, in each simulation one-third of a VBS bin was allowed to react. To see how this assumption affects model results, we made additional simulations where we allowed all molecules of a bin to react. The growth of the

particle in these simulations is presented in Figure 7b. The possible contribution of oligomerization or decomposition reaction
415   is remarkable. If only one-third of a bin was allowed to react the growth rate of the particle was in maximum increased by
oligomerization 71% and decreased 26% by decomposition, but if whole bin reacted, the maximum increase was 138% and
decrease 80%.

4. Conclusions

A wide range of model simulations were conducted to study effect of particle phase oligomerization and decomposition on the
420   nanoparticle growth. Based on our model results, these reactions have potential to affect particle growth. However, the extent
of the effect was strongly dependent on the assumed properties of the organics (volatilities of the initial and product
compounds, reaction rate coefficients and fraction of molecules that are reactive) and the sensitivity of particle growth on one
property depended on the other properties. In the simulations constrained by observed gas phase concentrations, the agreement
between simulated and observed particle growth rate changed considerably when the assumptions of the organic properties
425   were varied. However, simulated and observed growth rate can be brought to a good agreement with multiple combinations of
assumptions of the properties which would make it challenging to try to estimate which combination describes the condensing
organic properties best.

When considering agreement between observation constrained growth model simulations and observations of particle growth,
uncertainties in gas phase concentration measurements and in estimation of saturation vapor pressure of organics need to be
430   considered. For example, the C^* values vary over several orders of magnitude between different parametrizations (Mohr et al.,
2019) and there are discrepancies in C^* of organics bases on different measurement techniques (Bilde et al., 2015). Mohr et
al. (2019) estimated the uncertainty for gas phase concentrations of organics, which were same as used in our study, to be 53%
and considered an uncertainty of two orders of magnitude for saturation concentrations. In their model simulations these
uncertainty limits lead to 46% and 64% increase and 41% and 27% decrease in growth rates for uncertainties in gas phase
435   concentrations and saturation vapor pressures respectively. Compared to 71% increase by oligomerization and 26% decrease
by decomposition calculated in our study if one-third of a bin is allowed to react, these effects are similar in magnitude, but if
whole bin is allowed to react, the effect by oligomerization and decomposition are greater.

Within uncertainties, it is possible to explain the detected atmospheric nanoparticle growth based on the observed gas phase
concentrations even without particle phase oligomerization and decomposition, as shown by Mohr et al. (2019) and our base
440   case simulation. Nevertheless, oligomers are found in abundance in SOA and although some of it is oligomers condensed
straight from the gas phase, it is presumable that also particle phase oligomerization and decomposition occur as have been
shown by multiple studies (e.g. Zhao et al, 2005; Zhao et al., 2006; Krizner at al., 2009 and Wang et al., 2010). Hence, it
remains open to what extent particle phase reactions take place in nanoparticles and how much is particle growth rate affected
by them. Our results suggest that including these processes in models that describe atmospheric particle dynamics may be
445   required, however, as the simulated growth is sensitive to the assumptions of reactions and reaction rates, also investigations

to determine the exact properties are needed for this development to lead to more accurate model representation of the nanoparticle growth.

It is evident that oligomerization, if taking place in particle phase, increases particle growth rate, making it easier for them to reach large enough size to act as CCN. For instance, survival probability of particles from 3 nm to 20 nm calculated for the

450 NPF event presented in Fig. 7 were 15 %, 25 % and 44 %, respectively, when using the GR from the slowest growing, base case and fastest growing simulation among the ones where one-third of a bin could react. The competition between growth and scavenging is of crucial importance, when considering survival probability, especially at the smallest sizes as the coagulation sink decreases rapidly with growing particle size. On the other hand, due to Nano-Köhler effect the growth rate is also typically enhancing as a function of size (Kulmala et al., 2004). However, although particle's ability to act as CCN is

455 strongly dependent on size, that is not the only affecting factor, as it depends also on particle hygroscopicity (Köhler, 1936; Giordano et al., 2015). Oligomerization decreases particle hygroscopicity (Xu et al., 2014), which raises a question of how do these two effects, increase in growth rate and decrease in hygroscopicity, compare to each other considering cloud formation. This is an interesting and important topic of study for the future. In our simulations the molar fraction of oligomers was at maximum 18% for simulations where one-third of a bin was allowed to react and 27% in simulations where whole bin was

460 allowed to react. Further modeling studies are needed to simulate the parameter space in different environments and explore the competing processes in nanoparticle growth towards CCN sizes. These models require comprehensive aerosol and gas phase measurements to provide data to evaluate the performance of the models in different atmospheric environments.

Code availability: Codes are available from the corresponding author upon request.

465 *Data availability:* The data used in the study is published in Mohr et al. (2019).

Author contribution: AH and TY designed the study, AH developed the code and conducted the simulations, FL, JT, TP and MK planned and performed the measurements, AH, KL and TY analyzed the results, AH and TY prepared the manuscript with contribution from all co-authors.

Competing interests: The authors declare that they have no conflict of interest.

470 *Acknowledgements:* This work was supported by the Academy of Finland Center of Excellence programme (grant no. 307331), the Academy of Finland Flagship funding (grants no. 337550 and 337549), the Academy of Finland (projects no. 1325656, 299544, 316114 and 325647), "Quantifying carbon sink, CarbonSink+ and their interaction with air quality" INAR project funded by Jane and Aatos Erkko Foundation and European Research Council (ERC) project ATM-GTP (Contract No. 742206), Technical and scientific staff in Hyytiälä station are acknowledged. JAT and FLH were supported by grants from the U.S.

475 Department of Energy's Atmospheric System Research Program (DE-SC0011791 and DE-SC0021097)

References

Bilde, M., Barsanti, K., Booth, M., Cappa, C. D., Donahue, N. M., Emanuelsson, E. U., McFiggans, G., Krieger, U. K., Marcolli, C., Topping, D., Ziemann, P., Barley, M., Clegg, S., Dennis-Smither, B., Hallquist, M., Hallquist, A. M., Khlystov, A., Kulmala, M., Mogensen, D., Percival, C. J., Pope, F., Reid, J. P., Ribeiro da Silva, M. A. V., Rosenoern, T., Salo, K., Soonsin, V., Yli-Juuti, T., Prisle, N. L., Pagels, J., Rarey, J., Zardini, A. A., and Riipinen, I.: Saturation vapor pressures and transition enthalpies of low-volatility organic molecules of atmospheric relevance: from dicarboxylic acids to complex mixtures, Chem. Rev., 115, 4115–4156, 2015.

Boucher, O., Randall, D., Artaxo, P., Bretherton, C., Feingold, G., Forster, P., Kerminen, V.-M., Kondo, Y., Liao, H., Lohmann, U., Rasch, P., Satheesh, S. K., Sherwood, S., Stevens, B., and Zhang, X.Y.: Clouds and Aerosols. In: Climate Change 2013: The Physical Science Basis. Contribution of Working Group I to the Fifth Assessment Report of the Intergovernmental Panel on Climate Change [Stocker, T.F., Qin, D., Plattner, G.-K., Tignor, M., Allen, S. K., Boschung, J., Nauels, A., Xia, Y., Bex, V., and Midgley, P. M. (eds.)]. Cambridge University Press, Cambridge, United Kingdom and New York, NY, USA, 2013.

http://www.aim.env.uea.ac.uk

Clegg, S. L., Pitzer, K. S., and Brimblecombe, P.: Thermodynamics of multicomponent, miscible, ionic solutions. 2. Mixtures including unsymmetrical electrolytes, J. Phys. Chem., 96, 9470–9479,1992.

Clegg, S. L. and Seinfeld, J. H.: Thermodynamic models of aqueous solutions containing inorganic electrolytes and dicarboxylicacids at 298.15 K. 1. The acids as non-dissociating components, J. Phys. Chem. A, 110, 5692–5717, 2006a.

Clegg, S. L. and Seinfeld, J. H.: Thermodynamic models of aqueous solutions containing inorganic electrolytes and dicarboxylicacids at 298.15 K. 2. Systems including dissociation equilibria, J. Phys. Chem. A, 110, 5718–5734, 2006b.

D'Ambro, E. L., Schobesberger, S., Zaveri, R. A., Shilling, J. E., Hwan Lee, B., Lopez-Hilfiker, F. D., Mohr, C., and Thornton, J. A.: Isothermal Evaporation of α-Pinene Ozonolysis SOA: Volatility, Phase State, and Oligomeric Composition, ACS Earth Space Chem., 2, 1058−1067, 2018.

Dal Maso, M., Kulmala, M., Riipinen, I., Wagner, R., Hussein, T., Aalto, P. P., & Lehtinen, K. E. J.: Formation and growth of fresh atmospheric aerosols: eight years of aerosol size distribution data from SMEAR II, Hyytiälä, Finland. Boreal Environment Research, 10(5), 323-336, 2005.

Denkenberger, K. A., Mofet, R. C., Holecek, J. C., Rebotier, T. P., and Prather, K. A.: Real-Time, Single-Particle Measurements of Oligomers in Aged Ambient Aerosol Particles, Environ. Sci. Technol., 41, 5439-5446, 2007.

Donahue, N. M., Epstein, S. A., Pandis, S. N., and Robinson, A. L.: A two-dimensional volatility basis set: 1. organic-aerosol mixing thermodynamics. Atmos. Chem. Phys. 11, 3303–3318, 2011.

Ehn, M., Petäjä, T., Aufmhoff, H., Aalto, P., Hämeri, K., Arnold, F., Laaksonen, A., and Kulmala, M.: Hygroscopic properties of ultrafine aerosol particles in the boreal forest: diurnal variation, solubility and the influence of sulfuric acid, Atmos. Chem. Phys., 7, 211–222, https://doi.org/10.5194/acp-7-211-2007, 2007.

Epstein, S. A., Riipinen, I., and Donahue, N. M.: A semiempirical correlation between enthalpy of vaporization and saturation concentration for organic aerosol. Environ. Sci. Technol. 44, 743–748, 2010.

Fuchs, N. A., and Sutugin, A. G.: Highly dispersed aerosols, Ann Arbor Science Publishers, London, 1970.

Gao, S., Keywood, M., Ng, N. L., Surratt, J., Varutbangkul, V., Bahreini, R., Flagan, R. C., and Seinfeld, J. H.: Low-Molecular-Weight and Oligomeric Components in Secondary Organic Aerosol from the Ozonolysis of Cycloalkenes and r-Pinene, *J. Phys. Chem.*, *108,* 10147-10164, 2004.

Giordano, M., Espinoza, C., and Asa-Awuku, A.: Experimentally measured morphology of biomass burning aerosol and its impacts on CCN ability, Atmos. Chem. Phys., 15, 1807–1821, https://doi.org/10.5194/acp-15-1807-2015, 2015.

Hall IV, W. A., and Johnston, M. V.: Oligomer Content of α-Pinene Secondary Organic Aerosol, Aerosol Science and Technology, 45:1, 37-45, DOI: 10.1080/02786826.2010.517580, 2011.

Hall IV, W. A., and Johnston, M. V.: Oligomer Formation Pathways in Secondary Organic Aerosol from MS and MS/MS Measurements with High Mass Accuracy and Resolving Power, J. Am. Soc. Mass Spectrom. , 23:1097Y1108, 2012.

Hallquist, M., Wenger, J. C., Baltensperger, U., Rudich, Y., Simpson, D., Claeys, M., Dommen, J., Donahue, N. M., George, C., Goldstein, A. H., Hamilton, J. F., Herrmann, H., Hoffmann, T., Iinuma, Y., Jang, M., Jenkin, M. E., Jimenez, J. L., Kiendler-Scharr, A., Maenhaut, W., McFiggans, G., Mentel, Th. F., Monod, A., Prévôt, A. S. H., Seinfeld, J. H., Surratt, J. D., Szmigielski, R., and Wildt, J.: The formation, properties and impact of secondary organic aerosol: current and emerging issues, Atmos. Chem. Phys., 9, 5155–5236, https://doi.org/10.5194/acp-9-5155-2009, 2009.

Hari, P., and Kulmala, M.: Station for measuring ecosystem-atmosphere relations (SMEAR II), Boreal Environ. Res., 10, 315–322, 2005.

Heaton, K. J., Dreyfus, M. A., Wang, S., and Johnston, M. V.: Oligomers in the early stage of biogenic secondary organic aerosol formation and growth, Environ. Sci. Technol., 41, 6129–6136, https://doi.org/10.1021/es070314n, 2007.

Häkkinen, S. A. K., Äijälä, M., Lehtipalo, K., Junninen, H., Backman, J., Virkkula, A., Nieminen, T., Vestenius, M., Hakola, H., Ehn, M., Worsnop, D. R., Kulmala, M., Petäjä, T., and Riipinen, I.: Long-term volatility measurements of submicron atmospheric aerosol in Hyytiälä, Finland, Atmos. Chem. Phys., 12, 10771–10786, https://doi.org/10.5194/acp-12-10771-2012, 2012.

Kerminen, V.-M., Paramonov, M., Anttila, T., Riipinen, I., Fountoukis, C., Korhonen, H., Asmi, E., Laakso, L., Lihavainen, H., Swietlicki, E., Svenningsson, B., Asmi, A., Pandis, S. N., Kulmala, M., and Petäjä, T.: Cloud condensation nuclei production associated with atmospheric nucleation: a synthesis based on existing literature and new results, Atmos. Chem. Phys., 12, 12037–12059, https://doi.org/10.5194/acp-12-12037-2012, 2012.

Kolesar, K. R., Chen, C., Johnson, D., and Cappa, C. D.: The influences of mass loading and rapid dilution of secondary organic aerosol on particle volatility, Atmos. Chem. Phys., 15, 9327–9343, https://doi.org/10.5194/acp-15-9327-2015, 2015.

Kourtchev, I., Giorio, C., Manninen, A., Wilson, E., Mahon, B., Aalto, J., Kajos, M., Venables, D., Ruuskanen, T., Levula, J., Loponen, M., Connors, S., Harris, N., Zhao, D., Kiendler-Scharr, A., Mentel, T., Rudich, Y., Hallquist, M., Doussin, J.-F.,

Maenhaut, W., Bäck, J., Petäjä, T., Wenger, J., Kulmala, M., and Kalberer, M.: Enhanced volatile organic compounds
545   emissions and organic aerosol mass increase the oligomer content of atmospheric aerosols, Sci. Rep., 6, 35038, https://doi.org/10.1038/srep35038, 2016.

Krizner, H. E., De Haan, D. O., and Kua, J.: Thermodynamics and kinetics of methylglyoxal dimer formation: A computational study. J. Phys. Chem. 113, 6994-7001, 2009.

Kulmala, M., Laakso, L., Lehtinen, K. E. J., Riipinen, I., Dal Maso, M., Anttila, T., Kerminen, V.-M., Hõrrak, U., Vana, M.,
550   and Tammet, H.: Initial steps of aerosol growth, Atmos. Chem. Phys., 4, 2553–2560, https://doi.org/10.5194/acp-4-2553-2004, 2004.

Kulmala, M., Kontkanen, J., Junninen, H., Lehtipalo, K., Manninen, H. E., Nieminen, T., Petäjä, T., Sipilä, M., Schobesberger, S., Rantala, P., Franchin, A., Jokinen, T., Järvinen, E., Äijälä, M., Kangasluoma, J., Hakala, J., Aalto, P. P., Paasonen, P., Mikkilä, J., Vanhanen, J., Aalto, J., Hakola, H., Makkonen, U., Ruuskanen, T., Mauldin, R. L. 3rd, Duplissy, J., Vehkamäki,
555   H., Bäck, J., Kortelainen, A., Riipinen, I., Kurtén, T., Johnston, M. V., Smith, J. N., Ehn, M., Mentel, T. F., Lehtinen, K. E., Laaksonen, A., Kerminen, V.-M., and Worsnop, D. R.: Direct observations of atmospheric aerosol nucleation, Science, 339(6122), 943-6, doi: 10.1126/science.1227385, 2013.

Kulmala, M., Petäjä, T., Ehn, M., Thornton, J., Sipilä, M., Worsnop, D. R., and Kerminen, V.-M.: Chemistry of atmospheric nucleation: On the recent advances on precursor characterization and atmospheric cluster composition in connection with
560   atmospheric new particle formation, Annu. Rev. Phys. Chem., 65, 21–37, https://doi.org/10.1146/annurev-physchem-040412-110014,2014.

Köhler, H.: The nucleus in and the growth of hygroscopic droplets, Trans. Faraday Soc., 32, 1152-1161, 1936.

Lambe, A. T., Ahern, A. T., Wright, J. P., Croasdale, D. R., Davidovits, P., and Onasch, T. B.: Oxidative aging and cloud condensation nuclei activation of laboratory combustion soot, J. Aerosol Sci., 79(Supplement C), 31–39,
565   doi:10.1016/j.jaerosci.2014.10.001, 2015

Lehtinen, K. E. J. and Kulmala, M.: A model for particle formation and growth in the atmosphere with molecular resolution in size, Atmos. Chem. Phys., 3, 251–257, doi:10.5194/acp-3-251-2003, 2003.

Li, Y., Pöschl, U., and Shiraiwa, M.: Molecular corridors and parameterizations of volatility in the chemical evolution of organic aerosols, Atmos. Chem. Phys., 16, 3327–3344, https://doi.org/10.5194/acp-16-3327-2016, 2016.

570   Li, Z., Tikkanen, O.-P., Buchholz, A., Hao, L., Kari, E., Yli-Juuti, T., and Virtanen, A.: Effect of Decreased Temperature on the Evaporation of α-Pinene Secondary Organic Aerosol Particles, ACS Earth Space Chem., 3, 12, 2775-2785, https://doi.org/10.1021/acsearthspacechem.9b00240, 2019.

Merikanto, J., Spracklen, D. V., Mann, G. W., Pickering, S. J., and Carslaw, K. S.: Impact of nucleation on global CCN, Atmos. Chem. Phys., 9, 8601–8616, https://doi.org/10.5194/acp-9-8601-2009, 2009.

575   Mohr, C., Thornton, J. A., Heitto, A., Lopez-Hilfiker, F. D., Lutz, A., Riipinen, I., Hong, J., Donahue, N. M., Hallquist, M., Petäjä, T., Kulmala, M., and Yli-Juuti, T.: Molecular identification of organic vapors driving atmospheric nanoparticle growth. *Nat. Commun.* **10,** 4442, https://doi.org/10.1038/s41467-019-12473-2, 2019.

Nieminen, T., Asmi, A., Dal Maso, M., Aalto, P. P., Keronen, P., Petäjä, T., Kulmala, M., and Kerminen, V-M.: Trends in atmospheric new-particle formation: 16 years of observations in a boreal-forest environment. *Boreal Environment Research*, 580 *19*(suppl. B), 191-214, 2014.

Paramonov, M., Kerminen, V.-M., Gysel, M., Aalto, P. P., Andreae, M. O., Asmi, E., Baltensperger, U., Bougiatioti, A., Brus, D., Frank, G. P., Good, N., Gunthe, S. S., Hao, L., Irwin, M., Jaatinen, A., Jurányi, Z., King, S. M., Kortelainen, A., Kristensson, A., Lihavainen, H., Kulmala, M., Lohmann, U., Martin, S. T., McFiggans, G., Mihalopoulos, N., Nenes, A., O'Dowd, C. D., Ovadnevaite, J., Petäjä, T., Pöschl, U., Roberts, G. C., Rose, D., Svenningsson, B., Swietlicki, E., Weingartner, 585 E., Whitehead, J., Wiedensohler, A., Wittbom, C., and Sierau, B.: A synthesis of cloud condensation nuclei counter (CCNC) measurements within the EUCAARI network, Atmos. Chem. Phys., 15, 12211–12229, https://doi.org/10.5194/acp-15-12211-2015, 2015.

Pennington, M. R., Bzdek, B. R., DePalma, J. W., Smith, J. N., Kortelainen, A.-M., Hildebrandt Ruiz, L., Petäjä, T., Kulmala, M., Worsnop, D. R., and Johnston, M. V.: Identification and quantification of particle growth channels during new particle 590 formation, Atmos. Chem. Phys., 13, 10215–10225, https://doi.org/10.5194/acp-13-10215-2013, 2013.

Pierce J. R., and Adams P. J.: Efficiency of CCN formation from ultrafine particles, Atmos. Chem. Phys., 7, 1367–1379, 2007.

Presto, A. A., and Donahue, N. M.: Investigation of alpha-pinene plus ozone secondary organic aerosol formation at low total aerosol mass, Environ. Sci. Technol., 40, 3536–3543, doi:10.1021/Es052203z, 2006.

Reddington, C. L., Carslaw, K. S., Stier, P., Schutgens, N., Coe, H., Liu, D., Allan, J., Browse, J., Pringle, K. J., Lee, L. A., 595 Yoshioka, M., Johnson, J. S., Regayre, L. A., Spracklen, D. V., Mann, G. W., Clarke, A., Hermann, M., Henning, S., Wex, H., Kristensen, T. B., Leaitch, W. R., Pöschl, U., Rose, D., Andreae, M. O., Schmale, J., Kondo, Y., Oshima, N., Schwarz, J. P., Nenes, A., Anderson, B., Roberts, G. C., Snider, J. R., Leck, C., Quinn, P. K., Chi, X., Ding, A., Jimenez, J. L., and Zhang, Q.: The Global Aerosol Synthesis and Science Project (GASSP) Measurements and Modeling to Reduce Uncertainty, Bull. Am. Meteor. Soc. 98, 1857–1877, 2017.

600 Renbaum-Wolff, L., Grayson, J. W., Bateman, A. P., Kuwata, M., Sellier, M., Murray, B. J., Shilling, J. E., Martin, S. T., and Bertram, A. K.: Viscosity ofα-pinene secondary organic mate-rial and implications for particle growth and reactivity, P. Natl. Acad. Sci. USA, 110, 8014–8019, 2013

Roldin, P., Eriksson, A. C., Nordin, E. Z., Hermansson, E., Mogensen, D., Rusanen, A., Boy, M., Swietlicki, E., Svenningsson, B., Zelenyuk, A., and Pagels, J.: Modelling non-equilibrium secondary organic aerosol formation and evaporation with the 605 aerosol dynamics, gas- and particle-phase chemistry kinetic multilayer model ADCHAM, Atmos. Chem. Phys., 14, 7953–7993, https://doi.org/10.5194/acp-14-7953-2014, 2014.

Shrivastava, M., Cappa, C. D., Fan, J., Goldstein, A. H., Guenther, A. B., Jimenez, J. L., Kuang, C., Laskin, A., Martin, S. T., Ng, N. L., Pätäjä, T., Pierce, J. R., Rasch, P. J., Roldin, P., Seinfeld, J. H., Shilling, J., Smith, J. N., Thornton, J. A., Volkamer, R., Wang J., Worsnop, D. R., Zaveri, R. A., Zelemyuk, A., and Zhang, Q.: Recent advances in understanding secondary organic 610 aerosol: Implications for global climate forcing, Rev. Geophys., 55, 509–559, 2017.

Stolzenburg, D., Fischer, L., Vogel, A., L., Heinritzi, M., Schervish, M., Simon, M., Wagner, A. C., Dada, L., Ahonen, L. R., Amorim, A., Baccarini, A., Bauer, P. S., Baumgartner, B., Bergen, A., Bianchi, F., Breitenlechner, M., Brilke, S., Buenrostro Mazon, S., Chen, D., DiasI, A., Draper, D. C., Duplissy, J., El Haddad, I., Finkenzeller, H., Frege, C., Fuchs, C., Garmash, O., Gordon, H., He, X., Helm, J., Hofbauer, V., Hoyle, C. R., Kim, C., Kirkby, J., Kontkanen, J., K ürten, A., Lampilahti, J.,
615 Lawler, M., Lehtipalo, K., Leiminger, M., Mai, H., Mathot, S., Mentler, B., Molteni, U., Nie, W., Nieminen, T., Nowak, J. B., Ojdanic, A., Onnela, A., Passananti, M., Petäjä, T., Qu él éver, L. L. J.,, Rissanen, M. P., Sarnela, N., Schallhart, S., Tauber, C., Tomé, A., Wagner, R., Wang, M., Weitz, L., Wimmer, D., Xiao, M., Yan, C., Ye, P., Zha, Q., Baltensperger, U., Curtius, J., Dommen, J., Flagan, R. C., Kulmala, M., Smith, J. N., Worsnop, D. R., Hansel, A., Donahue, N. M., and Winkler, P., M.: Rapid growth of organic aerosol nanoparticles over a wide tropospheric temperature range, PNAS,vol 115, 9122–912,
620 www.pnas.org/cgi/doi/10.1073/pnas.1807604115, 2018.

Tolocka, M. P., Jang, M., Ginter, J. M., Cox, F. J., Kamens, R. M., and Johnston, M. V.: Formation of Oligomers in Secondary Organic Aerosol, Environ. Sci. Technol., 38, 1428-1434, 2004.

Tritscher, T., Jurányi, Z., Martin, M., Chirico, R., Gysel, M., Heringa, M. F., DeCarlo, P. F., Sierau, B., Prévôt, A. S. H., Weingartner, E., and Baltensperger, U.: Changes of Hygroscopicity and Morphology During Ageing of Diesel Soot, Environ.
625 Res. Lett., 6, 034026, https://doi.org/10.1088/1748-9326/6/3/034026, 2011.

Trump, E. R., and Donahue, N. M.: Oligomer formation within secondary organic aerosols: equilibrium and dynamic considerations, Atmos. Chem. Phys., 14, 3691–3701, https://doi.org/10.5194/acp-14-3691-2014, 2014.

Vesterinen, M., Lehtinen, K. E. J., Kulmala, M., and Laaksonen, A.: Effect of particle phase oligomer formation on aerosol growth, Atmospheric Environment 41 1768–1776, 2007.

630 Virtanen, A., Joutsensaari, J., Koop, T., Kannosto, J., Yli-Pirilä, P., Leskinen, J., Mäkela, J. M., Holopainen, J. K., Pöschl, U., Kulmala, M., Worsnop, D. R., and Laaksonen, A.: An amorphous solid state of biogenic secondary organic aerosol particles, Nature, 467, 2010.

Wang., L., Khalizov, A., F., Zheng, J., Xu, W., Ma, Y., Lal, V., and Zhang, R.: Atmospheric nanoparticles formed from heterogeneous reactions of organics, Nat. Geo. Sci., 3, DOI: 10.1038/NGEO778, 2010.

635 Wehner, B., Petäjä, T., Boy, M., Engler, C., Birmili, W., Touch, T., Wiedensohler, A., and Kulmala, M.: The contribution of sulfuric acid and non-volatile compounds on the growth of freshly formed atmospheric aerosols, Geophys. Res. Lett., 32, L17810, doi:10.1029/2005GL023827, 2005.

Wexler, A. S., and Clegg, S. L.: Atmospheric aerosol models for systems including the ions H^+, NH^+_4, Na^+, SO^2-_4, NO^-_3, Cl^-, Br^- and H_2O, J. Geophys. Res., 107, 4207, doi:10.1029/2001JD000451, 2002.

640 Xu, W., Guo, S., Gomez-Hernandez, M., Zamora, M. L., Secrest, J., Marrero-Ortiz, W., Zhang, A. L., Collins, D. R., and Zhang, R.: Cloud forming potential of oligomers relevant to secondary organic aerosols, Geophys. Res. Lett., 41, 6538–6545, doi:10.1002/2014GL061040, 2014.

Yli-Juuti, T., Nieminen, T., Hirsikko, A., Aalto, P. P., Asmi, E., Hõrrak, U., Manninen, H. E., Patokoski, J., Dal Maso, M., Petäjä, T., Rinne, J., Kulmala, M., and Riipinen, I.: Growth rates of nucleation mode particles in Hyytiälä during 2003−2009:

645   variation with particle size, season, data analysis method and ambient conditions, Atmos. Chem. Phys., 11, 12865–12886, https://doi.org/10.5194/acp-11-12865-2011, 2011.

Yli-Juuti, T., Barsanti, K., Hildebrandt Ruiz, L. Kieloaho, A.-J., Makkonen, U., Petäjä, T., Ruuskanen, T., Kulmala, M., and Riipinen, I.: Model for acid-base chemistry in nanoparticle growth (MABNAG). Atmos. Chem. Phys. 13, 12507–12524, 2013.

650   Yli-Juuti T., Tikkanen O.-P., Manninen H.E., Nieminen T., and Kulmala M.: Analysis of sub-3 nm particle growth in connection with sulfuric acid in a boreal forest. Boreal Env. Res. 21: 287–298, 2016.

Yli-Juuti, T., Pajunoja, A., Tikkanen, O.-P., Buchholz, A., Faiola, C., Väisänen, O., Liqing, H., Kari, E., Peräkylä, O., Garmash, O., Shiraiwa, M., Ehn, M., Lehtinen, K., and Virtanen, A.: Factors controlling the evaporation of secondary organic aerosol from α-pinene ozonolysis. Geophys. Res. Lett., 44, 2562–2570, doi:10.1002/2016GL072364, 2017.

655   Yli-Juuti, T., Mohr, C., and Riipinen, I.: Open questions on atmospheric nanoparticle growth, Comminucations Chemistry, 3:106, https://doi.org/10.1038/s42004-020-00339-4, 2020.

Zhang, R., Khalizov, A. F., Pagels, J., Zhang, D., Xue, H., and Mc-Murry, P. H.: Variability in morphology, hygroscopicity, and op-tical properties of soot aerosols during atmospheric processing, PNAS, 105(30), 10291–10296, doi:10.1073/pnas.0804860105,2008.

660   Zhao, J., Levitt, N. P., and Zhang, R. Heterogeneous chemistry of octanal and 2,4-hexadienal with sulfuric acid. Geophys. Res. Lett. 32, L09802, 2005.

Zhao, J., Levitt, N. P., Zhang, R., and Chen, J. Heterogeneous reactions of methylglyoxal in acidic media: Implications for secondary organic aerosol formation. Environ. Sci. Technol. 40, 7682-7687, 2006.

665